POINT DEFECTS IN BINARY LAVES-PHASE ALLOYS

J. H. Zhu[a,b], L. M. Pike[a], C. T. Liu[a], and P. K. Liaw[b]

[a] Metals and Ceramics Division, Oak Ridge National Laboratory, Oak Ridge, TN 37831-6115; [b] Department of Materials Science and Engineering, The University of Tennessee, Knoxville, TN 37996

ABSTRACT

Point defect mechanisms in the binary C15 $NbCr_2$ and $NbCo_2$, and C14 $NbFe_2$ systems on both sides of stoichiometry was studied and clarified by both bulk density and X-ray lattice parameter measurements. It was found that the vacancy concentrations in these systems after quenching from 1000°C are essentially zero. The constitutional defects on both sides of stoichiometry for these systems were found to be of the anti-site type in comparison with the model predictions. However, thermal vacancies exhibiting a maximum at the stoichiometric composition were obtained in $NbCr_2$ Laves phase alloys after quenching from 1400°C. These could be completely eliminated by annealing at 1000°C. Anti-site hardening was found on both sides of stoichiometry for all three Laves phase systems studied. Furthermore, the thermal vacancies in $NbCr_2$ alloys after quenching from 1400°C were found to soften the Laves phase. The anti-site hardening of the Laves phases is similar to that of the B2 compounds, while the thermal vacancy softening is unique to the Laves phase. Both the anti-site defects and thermal vacancies do not significantly affect the fracture toughness of the Laves phases.

DISCLAIMER

DISCLAIMER

Portions of this document may be illegible in electronic image products. Images are produced from the best available original document.

1. INTRODUCTION

Laves phases of AB_2 composition are a common type of topologically close-packed (TCP) structures, with three polytypes most frequently observed: cubic C15, hexagonal C14 and dihexagonal C36 [1-4]. These phases are generally considered to be line compounds at a strict AB_2 composition. However, solubility ranges exist for about 25% of the known binary Laves phases [5]. For non-stoichiometric compositions, constitutional defects are incorporated into intermetallic compounds. However, for the Laves phases, little is known about the possible defect structures that may be associated with the solubility at off-stoichiometric compositions. The excess atoms in off-stoichiometric compounds can stay on their own sublattice, leading to the formation of constitutional vacancies on the other sublattice, insert into interstitial sites, or occupy sites on the other sublattice (anti-site substitution). Since Laves phases have TCP structures and space-filling is relatively high, there are no interstitial sites with a comparable size to that of the component atoms. Therefore, the insertion of the excess atoms into the interstitial sites can be excluded, and the possible defect mechanisms reduce to either constitutional vacancy or anti-site substitution for binary Laves phases.

The Laves phases are known to be size compound, i.e., the atomic size ratio, R_A/R_B is ideally 1.225, with a range of 1.05 to 1.67 typically observed. Based on geometric arguments, it has been postulated that the A-rich side is accommodated by vacancies, while the B-rich compositions result from the anti-site substitution [5]. Since the A atom is much larger than B atom, the excess A atoms in A-rich compositions would tend to stay on their own sublattice sites, thus creating vacancies on the B atom sublattice. On the other hand, the excess B atoms on B-rich compositions would be able to occupy the A atom sublattice sites, leading to the formation of anti-site defects. These postulations are based on geometric considerations, and no systematic experimental verification has been undertaken so far.

The types of constitutional defects may affect physical, mechanical and functional properties of Laves phases. Vacancies have been proposed to assist the movement of synchro-Shockley dislocations [6], thus possibly facilitating the synchroshear deformation mechanism and increasing the toughness of Laves phases [7]. Off-stoichiometry was also found to affect the hydride stability of $ZrMn_2$ [8] and the hydrogen storage capability of $TiMn_2$ alloys [9].

The $NbCr_2$ Laves phase has received considerable attention recently as a potential high-temperature structural material [10-13], due to its high melting temperature (1730°C), appreciable creep resistance, high strength, relatively low density (7.7 g/cm^3), and good oxidation resistance below 1100°C. It has a limited range of solubility on both sides of stoichiometry. The geometric factor [5] and electronic factor [14] have been cited to contribute to such a solubility range. Our preliminary results indicate that anti-site substitution is the defect mechanism on both sides of stoichiometry in $NbCr_2$ Laves phase [15]. However, more systematic study should be undertaken to investigate the off-stoichiometric defects in this binary system, since such information is imperative in understanding the phase stability, deformation characteristics, and alloying behavior of the Laves phase alloy.

The $NbCo_2$ Laves phase has been selected as a model material for studying off-stoichiometric defects. Saito and Beck [16] performed a comparison of the X-ray density with gravimetrically measured densities for the Co-rich $NbCo_2$ Laves phase system. Their measurements show that the variable stoichiometry of the $NbCo_2$ Laves phase is the result of the progressive occupation of Nb sites by Co atoms, with no indication of the formation of constitutional vacancies in the Nb sublattice. Note that only the Co-rich side was studied previously, and only qualitative information regarding the defect mechanism is available. From the geometric considerations, such anti-site substitution is expected for the Co-rich side. However, a more interesting study would be to clarify the constitutional defect

mechanisms on the Nb-rich side, which may be constitutional vacancies according to the previous reasoning. So far, no work has been conducted to carefully determine the homogeneity range of this Laves phase, especially the Nb-rich side. No solubility has been indicated on the Nb-rich side of this Laves phase system from the Nb-Co phase diagram [17]. The solubility range and the possible defect mechanisms on the Nb-rich side in this system will be carefully determined in this study.

While the $NbCr_2$ and $NbCo_2$ Laves phases are of a cubic C15 structure, the third Laves phase system to be studied, $NbFe_2$, has a hexagonal C14 structure. The homogeneity range of this Laves phase has been investigated by Smith, Rogers and Rawlings [18], Paul and Swartzendruber [19] and more recently by Bejarano et al. [20]. The homogeneity range was originally thought to be from 27 to 38 at.% Nb [19], but should be much narrower, i.e., from 32 to 37 at.% Nb, according to the recent study [20]. From the lattice parameter measurements, the defect mechanism has been postulated to be anti-site substitution for both the Fe-rich and Nb-rich sides [18]. Furthermore, the authors postulated that there may be thermal vacancies existing in the stoichiometric compound. However, no direct measurement of the vacancy concentration in this Laves phase has been undertaken so far.

In the present study, we have attempted to clarify the point defect mechanisms on both sides of stoichiometry in these three binary systems, by measuring the lattice parameters, bulk densities, and therefore, vacancy concentrations of binary $NbCr_2$, $NbCo_2$, and $NbFe_2$ alloys of various compositions after quenching from 1000°C. For the $NbCr_2$ alloys, the vacancy concentrations after quenching from 1400°C were also determined to observe whether thermal vacancies can be introduced by quenching from elevated temperatures.

The hardness of the above alloys with various point defect concentrations was determined in an attempt to explore the solid solution hardening behavior in the Laves

phases. The fracture toughness was also measured to investigate if the point defects affect the toughness of the alloys, and, in particular, to see if vacancies facilitate synchroshear deformation in the vacancy-containing alloys.

2. EXPERIMENTAL PROCEDURES

The alloy compositions investigated in this study are listed in Tables I, II, and III. A total of 19 binary alloys were prepared: 6 for the $NbCr_2$ system, 6 for the $NbCo_2$ system, and 7 for the $NbFe_2$ system. For each alloy system, the Nb content in the alloy increases with the code number. The selected compositions covered a wide range of stoichiometry: for $NbCr_2$ and $NbCo_2$ systems, alloys #1 - 3 are Cr-rich or Co-rich, and #4 is the stoichiometric alloy, while alloys #5 and #6 are Nb-rich; for the $NbFe_2$ system, alloys #1 - 2 are Fe-rich and #3 is the stoichiometric one, while alloys #4 - 7 are Nb-rich. Ingots of approximately 50 grams were prepared by arc-melting techniques using high-purity starting materials. According to our melting experience, an excess amount (typically 0.05 gram) of Cr was added to compensate for the evaporation loss of Cr during melting for the $NbCr_2$ alloys. Each ingot was remelted at least 5 times to ensure compositional homogeneity.

All the alloys were given a homogenization anneal of 1300°C for 10 hours in vacuum, except the alloys #1 and #2 of the $NbCo_2$ system which were homogenized at 1200°C for 24 hours in vacuum because of their relatively low-melting temperatures. After the homogenization anneal, all the alloys were sectioned into two halves. One half was encapsulated in quartz, which was evacuated and backfilled with helium and heat-treated at 1000°C for 7 days, followed by water quenching. The other half of the 6 alloys in the binary $NbCr_2$ system was heat-treated at 1400°C for 1 hour in a vertical flowing-argon furnace, then water quenched. All the alloys were fully homogenized following the above heat treatments, except the alloys #1 and #2 for the $NbCo_2$ system. Therefore, density and vacancy concentration measurements were not conducted for these two alloys.

Small fractions of the quenched samples were mounted for microstructural observations, and chemical composition analyses of the various phases in the heat-treated condition, using an optical microscope and a field-emission-gun scanning electron microscope (SEM) equipped with an energy dispersive X-ray spectroscope (EDS).

The remaining parts of the samples were crushed into powders in an agate mortar with particle sizes smaller than 40 mesh. Powders with a mesh size of -40+80 were used for bulk density measurements, and powders smaller than 320 mesh were used for X-ray analyses. The bulk density was measured using a helium pycnometer with an accuracy of approximately 0.01 vol.%. The use of powdered samples was intended to eliminate the micropores generated during solidification, and thus, will lead to more accurate density measurements. The vacancy concentration of the Laves-phase alloys, c_v, which is defined as the ratio of the total number of vacancies to the total number of atoms, can be obtained from the following equation:

$$c_V = \frac{\rho_X - \rho_B}{\rho_B} \qquad (1)$$

where ρ_X and ρ_B are the X-ray and the bulk densities, respectively.

X-ray diffraction measurements were made using a Scintag XD2000 diffractometer with Cu K_a radiation. The lattice parameter was determined from 13-15 peaks. The X-ray density was calculated using the measured lattice parameter. The accuracy of the vacancy concentration using our method is approximately 0.08%, which is mainly due to the compositional uncertainty of the alloys.

The microhardness was measured on a Buehler microhardness tester using a load of 50 grams with a holding time of 15 seconds. Due to the extremely brittle nature of the Laves phases, it is challenging to determine the hardness and discern the hardness difference for the Laves phases with small compositional variations. The use of 500 gram loads leads to the extensive cracking near the corners of the indented region, which makes

the determination of the diagonal length less accurate. Therefore, a smaller load of 50 grams was chosen for indentation, which tends to reduce the cracking problem and make the measurement of the diagonal length more accurate. Due to the small size of the indents, a scanning electron microscope with a field-emmision gun was used to measure the diagonal lengths with a high magnification of 10,000x. The magnification of the SEM was calibrated with a calibration grating. The Vickers hardness number (VHN) is determined by the following equation [21]:

$$VHN = \frac{1.854P}{L^2} \tag{2}$$

where P = applied load (kg) and L = average length of diagonals (mm).

The fracture toughness of the alloys was calculated from the crack length values after indentation using a load of 500 g with a holding time of 15 seconds. The crack lengths were measured immediately after the indentation to eliminate the possibility of slow crack propagation following the removal of the indenter. The following equation was used to calculate the fracture toughness of the alloy [22, 23]:

$$K_{IC} = A\left(\frac{E}{H}\right)^n \frac{P}{L^{3/2}} \tag{3}$$

where K_{IC} = fracture toughness ($MPa\sqrt{m}$), E = Young's modulus (GPa), which is assumed to be 218 GPa for all of the investigated alloys, H = Vickers hardness (GPa), P = load (N), and L = average length of the four radial cracks from the center of the indent to the crack tip. A and n are constants, which are taken as 0.016 and 0.5, respectively, for relatively brittle materials [22].

3. RESULTS

3.1 Microscopic Observation

Optical microstructural observations show that for the $NbCr_2$ Laves phase system the alloys #2 - 6 listed in Table 1 are in the single Laves phase region, and alloy #1 is in the

two-phase region after quenching from 1400°C. After quenching from 1000°C, the alloys #3 - 6 are in the single Laves phase region and alloys #1 and #2 are in the two-phase region. Alloy #1 after quenching from 1400°C and alloy #2 after quenching from 1000°C retain small amounts of a second phase. Such observations are further supported by the lattice parameter results, as shown later. Typical microstructures of single Laves phase alloys, which were etched with a solution of $HF:HNO3:H_2O$ = 1:1:3, are shown in Fig. 1 (a). There are many annealing twins in the alloy, indicating that the C15 structure is easily twinned, i.e., it has a low stacking fault energy. The second phase in alloys #1 and #2 was analyzed with EDS in an SEM, and determined to be a Cr solid solution with a small amount of Nb. Figure 1 (b) presents an SEM micrograph of alloy #1 after quenching from 1000°C, with a two-phase microstructure. The dark phase and the matrix are the Cr phase and $NbCr_2$ Laves phase, respectively, as is clear from the EDS results shown in Fig.1 (c). The maximum solubility of Cr in $NbCr_2$ at 1000°C in this study is found to be similar to the value reported in the recent binary Cr-Nb phase diagram [14].

For the $NbCo_2$ system, all the alloys except #6 are within the homogeneity range, and there are few annealing twins in the alloys, as compared to the $NbCr_2$ alloys, indicating the stacking fault energy is higher in this $NbCo_2$ phase. Figure 2 (a) shows the optical microstructure of the stoichiomteric $NbCo_2$ alloy, etched with a solution of 60% glycerine + 20% HNO_3 + 10% HF +10%H_2O (in vol.%). The alloys #1 and #2 are not fully homogenized. The alloy #6 is in the two-phase range, i.e., there are small amounts of second phase, especially near grain boundaries, see Fig. 2 (b). The second phase is β Nb_6Co_7 phase, with a $D8_5$ structure, according to the binary Nb-Co phase diagram [17]. Consistent with the phase diagram, the EDS results show that this phase is richer in Nb content than the matrix. Compared with the binary Nb-Co phase diagram where no

solubility on the Nb-rich side is indicated, it was found that the solubility of Nb in the $NbCo_2$ Laves phase is higher than 0.5 at.%, but less than 1 at.%.

For the $NbFe_2$ system, the alloys #1 - 5 are within the homogeneity range, and alloys #6 and #7 are in the region of two phases, $NbFe_2$ Laves phase and NbFe μ phase [20]. Figure 3 (a) shows the microstructure of a single-phase stoichiomteric $NbFe_2$ alloy, with large grains and no annealing twin. Figure 3 (b) shows the two-phase structures in alloy #7, and the EDS results indicate the second phase is richer in Nb than the matrix. Compared to the binary Nb-Fe phase diagram [20], the maximum solubility of Nb in $NbFe_2$ at 1000°C in this study (~35 at.%) is found to be lower than the reported one (37 at.% Nb).

3.2 Lattice Parameter, Density, and Vacancy Concentration

3.2.1 Binary $NbCr_2$ Alloys

The lattice parameters of the C15 $NbCr_2$ alloys listed in Table I are plotted in Fig. 4 as a function of stoichiometry for all the samples quenched from both 1400°C and 1000°C. As the Nb content increases, the lattice parameter of the $NbCr_2$ phase also increases. For the alloys quenched from 1400°C, the data points for the Cr-rich side fit along a straight line; similarly, for the Nb-rich side, the data points also fit along a straight line, with a slope greater than that of the line on the Cr-rich side. For the alloys quenched from 1000°C, similar trends are observed, except that on the Cr-rich side the lattice constants are identical for alloys #1 and #2, which indicates the composition of the Laves phase is the same in the two alloys. This is expected, because these two alloys were found to be in the two-phase region. Except for alloy #1, the lattice parameters after quenching from 1000°C are similar to those after quenching from 1400°C.

The X-ray and bulk density results after quenching from both 1400°C and 1000°C for $NbCr_2$ alloys are presented in Table I and Fig. 5. The density of the alloys increases as

the Nb content increases. Also, the bulk densities after quenching from 1000°C are consistently higher than those after quenching from 1400°C. Using Eq. 1 and the data presented in Table I and Fig. 5, the vacancy concentrations were calculated, and are also listed in Table I. Due to the presence of the second phase, the vacancy concentration could not be determined for alloy #1 after quenching from 1400°C, and alloys #1 and #2 after quenching from 1000°C. Figure 6 is a plot of the vacancy concentration as a function of the Nb content for the single-phase alloys after quenching from both 1400°C and 1000°C. It is interesting to note that the vacancy concentration in the alloys is quite high after quenching from 1400°C, which reaches a peak (~ 0.33 %) at the stoichiometric composition and decreases on both sides of stoichiometry. After annealing at 1000°C, the vacancies are annealed out and the vacancy concentrations are near zero (considering the accuracy of the vacancy concentration measurements). However, a slight peak at the stoichiometric composition can still be detected.

3.2.2 Binary $NbCo_2$ Alloys

The lattice parameters of the C15 $NbCo_2$ alloys listed in Table II are plotted in Fig. 7 as a function of stoichiometry for the samples quenched from 1000°C. As the Nb content increases, the lattice parameter of the $NbCo_2$ phase also increases. The data points for the Cr-rich side fit along a straight line; for the Nb-rich side, the initial data points also fit along a straight line, with a slope greater than that of the line on the Cr-rich side, similar to the result observed in $NbCr_2$ alloys (Fig. 4). The lattice parameter of alloy #6 does not fit along the line, due to the two-phase nature of this alloy. The solubility of Nb in $NbCo_2$ is about 34 at.%, see Fig. 7.

The X-ray and bulk density results for the $NbCo_2$ alloys after quenching from 1000°C are presented in Table II and Fig. 8. Both the X-ray and bulk densities of the alloys increase initially as the Nb content increases; however, on the Nb-rich side, the X-

ray and bulk densities of the alloys decrease slightly as the Nb content increases. Such decrease in the bulk density with the increase of the Nb content is different from the $NbCr_2$ system (Fig. 5), indicating that there may be a great amount of vacancies genrated in these alloys, therby reducing the alloydensity. Using Eq. 1 and the data presented in Table II and Fig. 8, the vacancy concentrations were calculated, and are also listed in Table II. The results indicate that the vacancy concentration in the alloys is quite low, i.e. essentially zero, considering the accuracy of the vacancy concentration measurement. No peak at the stoichiometric composition in the vacancy concentration can be discerned from these data. It is interesting to note that the decrease of the bulk density, as the content of the heavy element Nb in the alloy increases, does not necessarily mean that there are excess vacancies in the alloys. This is due to the fact that as Nb increses on the Nb-rich side, the lattice parameter increases significantly, leading to the reduction in X-ray density. As a result, no vacancies are generated by the simultaneous decrease in X-ray and bulk densities, according to Eq. 1.

3.2.3 Binary $NbFe_2$ Alloys

The lattice parameters of the C14 $NbFe_2$ alloys listed in Table III are plotted in Fig. 9 as a function of stoichiometry for all the $NbFe_2$ alloys quenched from 1000°C. Basically, as the Nb content increases, the lattice parameters, a and c, of the $NbFe_2$ compound also increase. The data points for the Fe-rich side fit roughly along a line; and for the Nb-rich side, a similar fitting is observed for the initial data points, with a slope greater than that of the line on the Fe-rich side. For the last two data points on the Nb-rich side, the lattice parameters, a and c, are both identical for alloys #6 and #7, indicating that the composition of the Laves phase is the same in the two alloys. This is expected, because these alloys are in the two-phase region from the microstructural observation. If we extrapolate the lines on the Nb-rich side to the a and c values for the alloys #6 and #7, the maximum solubility of Nb in the

$NbFe_2$ Laves phase is estimated to be around 35 at.%. This value is lower than the reported one (37 at.% Nb) [20].

The X-ray and bulk density results for the $NbFe_2$ Laves phases after quenching from 1000°C are presented in Table III and plotted in Fig. 10. Initially, the density of the alloys increases as the Nb content increases. However, after the Nb content reaches 33.8 at.%, the density decreases with a further increase in the Nb content. This is similar to what was observed in the $NbCo_2$ alloys. Also, the bulk densities after quenching from 1000°C are consistently smaller than the X-ray densities. Using Eq. 1 and the data presented in Table III and Fig. 10, the vacancy concentrations were calculated, and are also listed in Table III. Due to the presence of the second phase, the vacancy concentration could not be determined for alloys #6 and #7. The vacancy concentrations are essentially zero (considering the accuracy of the vacancy concentration measurements) for all the single-phase alloys. No peak at the stoichiometric composition in the vacancy concentration can be detected from the data in Table III.

3.3 Hardness and Fracture Toughness Behavior

The hardness as a function of the stoichiometry for the $NbCr_2$ alloys after quenching from 1400 and 1000°C is plotted in Fig. 11. It can be seen that as the composition deviates from the stoichiometry, the hardness of the Laves phase increases on both sides of stoichiometry. Since constitutional anti-site defects are the defect mechanisms on both Cr-rich and Nb-rich sides, anti-site substitution hardening was observed. Furthermore, the hardness of the alloys quenched from 1400°C is consistently lower than that of the alloys quenched from 1000°C, presumably due to the presence of thermal vacancies (Fig. 6). Such vacancy-induced softening of the materials is different from what was observed in B2 interemetallics, where the vacancy is a stronger hardener than the anti-site defect [25].

The hardness as a function of the stoichiometry for the $NbCo_2$ alloys quenched from 1000°C is plotted in Fig. 12. It can be seen that as the composition deviates from the stoichiometry, the hardness of the Laves phase increases, i.e., anti-site substitution hardening was observed. This is similar to the situation in the $NbCr_2$ Laves phases (Fig.11).

The hardness as a function of the stoichiometry for the $NbFe_2$ alloys quenched from 1000°C is plotted in Fig. 13. It can be seen that as the composition deviates from the stoichiometry, the hardness of the Laves phase increases, i.e., anti-site substitution hardening was observed again. Thus, anti-site substitutional hardening is observed for both C15 ($NbCr_2$ and $NbCo_2$) and C14 ($NbFe_2$) alloys, indicating that anti-site substitutional hardening may be a general phenomenon for Laves phase alloys.

The fracture toughness values as a function of the Nb content in $NbCr_2$ Laves phases after quenching from 1400°C and 1000°C as well as $NbCo_2$ and $NbFe_2$ Laves phases after quenching from 1000°C are plotted in Fig. 14. Basically, the fracture toughness of the $NbCr_2$ and $NbCo_2$ alloys is close to 1 $MPa.m^{1/2}$. No effect of stoichiometry on the fracture toughness can be discerned. Even though the presence of the anti-site defects hardens the Laves phase (Figs. 11 - 13), they are not detrimental to the fracture toughness of the alloy. Furthermore, it is noted that the fracture toughness of the $NbCr_2$ alloys after quenching from 1400°C is similar to that of the alloys after quenching from 1000°C, i.e., the presence of thermal vacancies does not lead to the improved toughness of the Laves phases, even though the vacancies slightly soften the Laves phases (see Fig. 11).

The fracture toughness of the C14 $NbFe_2$ alloys is lower than that of C15 $NbCr_2$ and $NbCo_2$. This trend can be explained by the fact that C15 structure is cubic, and is possibly more deformable than the hexagonal C14 structure. No effect of stoichiometry on the fracture toughness can be discerned. Again, even though the presence of the anti-site

defects hardens the Laves phase (Fig. 13), they are not detrimental to the fracture toughness of the alloy. Furthermore, it is noted that the fracture toughness of the two-phase alloys is higher than the single-phase alloys, which indicates that the μ phase may be tougher that the Laves phase.

4. DISCUSSION

4.1 Defect Mechanisms in Binary Laves Phases

The study of point defects in intermetallic compounds is an important topic. Defect mechanisms are closely related to physical and mechanical properties, such as diffusivity, hardness, ductility, etc. Many research efforts have been devoted to the elucidation of the defect types in B2 structures, such as FeAl and NiAl [25, 26]. For example, it is now generally accepted that the defects in the Ni-rich NiAl are of the anti-site type, i.e., the excess Ni will go to the Al sublattice site, while the excess Al in NiAl prefers to stay on its own sublattice, leading to the creation of vacancies on the Ni sublattice. Also, thermal vacancies can be easily generated in FeAl alloys by quenching from elevated temperatures [27], while the thermal vacancy concentration is much lower in NiAl [26] than in FeAl.

Previously, very limited studies have been undertaken to clarify the point defect mechanisms in Laves phases. Chen et al. [7] found from density measurements that both vacancy and anti-site defects are operating in the $TiCr_2$ Laves phase. Another study by Fleischer [28] found that anti-site substitution occurs on both sides of stoichiometry for the C15 $ZrCr_2$ Laves phase. Pargeter and Hume-Rothery [29] Saito and Beck [16] investigated the point defects in Co-rich $NbCo_2$ and $NbCo_3$ Laves phases and found that in both phases, the deviation from stoichiometry resulted from the substitution of Co atoms for the Nb atoms. However, constitutional defects on the Nb-rich side were not studied. X-ray and neutron diffraction measurements [30] showed that for both $ZrFe_2$ and $TiFe_2$, the excess Fe atoms are associated with the sites of Zr or Ti atoms. The concentration

variation of the lattice constants confirms such an anti-site substitution mechanism. The constitutional defect structure of the $NbFe_2$ Laves phase was also investigated by measuring the lattice parameters on both sides of stoichiometry, and again anti-site substitution was found to be the defect mechanism [18]. Off-stoichiometry in the YAl_2 Laves phase was postulated to be accompanied by different defect mechanisms: the Y-rich side is accommodated by vacancies, while the Al-rich compositions result from anti-site substitution [31]. From lattice parameter measurements of $NbCr_2$ Laves phases, Thoma et al. [5, 13] have postulated that constitutional vacancies on the Cr sublattice for the Nb-rich side of stoichiometry and anti-site substitution of Cr atoms on the Nb sites for the Cr-rich side of stoichiometry are probable defect mechanisms for $NbCr_2$ system. It should be noted that in all of the above studies, the alloy compositions were not carefully controlled and vacancy concentrations in the Laves phases were not determined. Thus, no definitive conclusions on the defect mechanisms could be made from those studies.

The shape of the lattice parameter versus composition curve can provide valuable insight on constitutional defect mechanisms. For example, this type of information has been used to successfully predict the constitutional defect mechanisms in a number of B2-ordered compounds [26]. These ideas can be extended to the present case by the consideration of Figs. 4, 7, and 9. The lattice parameters at the Cr, Co, or Fe-rich compositions increase with increasing Nb concentration. This is not surprising because Nb has a larger atomic size than Cr, Co, or Fe. However, on the Nb-rich side of stoichiometry, it is observed that the lattice parameter *increases* at an even greater rate with increasing Nb concentration for all these three Laves phase systems. This behavior suggests that the constitutional defect at Nb-rich compositions is Nb anti-site substitution. Only if a *decrease* in the rate of the lattice parameter change on the Nb-rich side of stoichiometry had been observed, would constitutional vacancies be a possibility.

The vacancy concentration results further confirm this conclusion unambiguously. The measured vacancy concentrations for all the single phase alloys after quenching from 1000°C are plotted in Fig. 15, together with the calculated vacancy concentrations from both the constitutional vacancy model and anti-site substitution model. The constitutional vacancy model is based on the assumption that all the excess atoms exclusively stay at their own sublattice, thus constitutional vacancies are created on the sublattice of the other element. The constitutional vacancy concentration values in Laves phases of different stoichiometries can be deduced from a simple calculation based on this model. The lattice site relationshiop $N^{\alpha} = 2N^{\beta}$, where N^{α} and N^{β} is the total numbers of sublattice sites of α (B sublattice) and β (A sublattice), holds for binary AB_2 Laves phases. Since both α and β sublattice can be occupied by A, B, or vacancy (Δ), we have

$$N_A^{\alpha} + N_B^{\alpha} + N_{\Delta}^{\alpha} = 2(N_A^{\beta} + N_B^{\beta} + N_{\Delta}^{\beta}) \qquad (4),$$

where N_A^{α} is the number of α lattice sites occupied by A atoms.

For the A-rich compound, assuming that constitutional vacancies are the only type of defects, we have

$$N_A^{\alpha} = N_B^{\beta} = N_{\Delta}^{\beta} = 0 \qquad (5).$$

Substituting Eq.(5) into Eq.(4), the following equation is obtained

$$N_B^{\alpha} + N_{\Delta}^{\alpha} = 2N_A^{\beta} \qquad (6).$$

Rearranging Eq.(6) and dividing both sides by N, we get

$$c_V = 2x_A - x_B \qquad (7).$$

Similarly, for the B-rich compound, the vacancy concentration can be expressed as

$$c_V = 0.5x_B - x_A \qquad (8).$$

From Eqs.(7) and (8), the constitutional vacancy model gives a vacancy concentration of zero at the stoichiometric composition, and the vacancy concentration increases on both sides of off-stoichiometry. The anti-site substitutional model assumes that the excess atoms occupy the sublattice sites of the other species. Thus, anti-stite defects

are created, and no constitutional vacancies are needed for the balance of the lattice sites. Obviously, the constitutional vacancy concentrations are zero for both A- and B-rich Laves phases, according to the anti-site substitutional model.

From Fig. 15, it is obvious that the measured vacancy concentrations for all the single-phase alloys after quenching from 1000°C are essentially zero (see also Tables I, II, and III), indicating that there are no constitutional vacancies in these Laves phases on either side of stoichiomtery. This is consistent with the anti-site substitution model and contrary to the constitutional vacancy model which demands much higher vacancy concentrations for off-stoichiometric compositions. Thus, the constitutional defects on both Cr-, Co-, or Fe-rich and Nb-rich sides of stoichiometry are of anti-site type for the $NbCr_2$, $NbCo_2$, and $NbFe_2$ Laves phases.

The atomic size ratio, R_A/R_B, of the AB_2 Laves phases studied in this paper can be calculated to be 1.145, 1.173, and 1.152 for $NbCr_2$, $NbCo_2$, and $NbFe_2$, respectively. Here, R_A and R_B are the atomic radii of the A and B atoms with a coordination number of 12 [32]. Obviously, all the Laves phases studied have R_A/R_B ratios smaller than the ideal ratio of 1.225 for Laves-phase formation. It will be interesting to know the defect mechanism for Laves phases with R_A/R_B greater than 1.225. It may be more possible to obtain constitutional vacancies for Laves phases with $R_A/R_B > 1.225$, due to geometric considerations, i.e., it is more difficult for A atoms to stay on the sublattice sites of B atoms as their atomic size difference increases.

4.2 Thermal Vacancy in Binary $NbCr_2$ Laves Phases

It is interesting that the measured vacancy concentration exhibits a maximum at the stoichiometric composition and decreases on both sides of stoichiometry for the $NbCr_2$ alloys when quenched from 1400°C (Fig. 6). Since these vacancies were essentially annealed out at 1000°C (see Fig. 6), and since the constitutional defects in this compound

have been established to be of the anti-site type, it is concluded that these defects are *thermal* vacancies. The shape of this curve may at first seem unique; however, a useful analog can be found when considering triple-defect B2 phases. This class of compounds has constitutional as well as thermal vacancies [26]. If the constitutional component is subtracted from the total vacancy concentration, it is found that the thermal vacancy concentration exhibits a maximum at the stoichiometric composition, as is the case in our $NbCr_2$ system. This behavior is exhibited by the NiGa and CoGa compounds, for example. A convenient summary of such data is found in the review by Chang and Neumann [26]. A maximum in thermal vacancy concentration at the stoichiometric composition can be rationalized by considering that the increase in entropy associated with the introduction of vacancies will be the greatest at the stoichiometric composition where the degree of order is necessarily the highest. An interesting problem in the future would be to determine whether the thermal vacancies sit on the Cr-site, the Nb-site, or both.

4.3 Solid Solution Hardening in Binary Laves Phases

A point defect in a crystalline lattice is well known to cause hardening. This phenomenon is referred to as solid solution hardening. Solid solution hardening has been extensively studied in B2 compounds [25]. Generally, it was found that in B2 compounds with anti-site defects, hardness exhibits a minimum at the stoichiometric composition, and deviation from stoichiometry causes hardening of the compounds, due to the presence of consitutional anti-site defects. For triple-defect B2 compounds, the shape of the hardness versus composition curves was found to be not so simple and depended on the degree of thermal disorder. Also, vacancies were found to be a more potent hardener than the anti-site defects.

In the three Laves phases we studied, the hardness was also found to have a characteristic V-shape with a minimum occurring at the stoichiometric compositions (Figs.

11 - 13). Obviously, similar to anti-site B2 compounds, such off-stoichiometric hardening can be attributed to the presence of constitutional anti-site defects, which are the defect mechanism on both sides of stoichiometry in these Laves phases. The anti-site hardening mechanism in Laves phases, however, is not clear so far, which must be different from that in B2 compounds. In B2 compounds, the anti-site hardening is ofeten correlated to an interaction between the stress filed of a moving dislocation and that of the anti-site defect; however, it is impossible for ordinary dislocations to move in Laves phases at ambient temperature.

The hardness values of all $NbCr_2$ alloys after quenching from 1400°C were found to be lower than those after quenching from 1000°C (Fig. 11). Since thermal vacancies are incorporated into the compound after quenching from 1400°C (see Fig. 6), the above results indicate that vacancies cause softening, instead of hardening of the $NbCr_2$ Laves phases. Such vacancy-induced softening is very unique and has not been observed previously. Furthermore, this is in direct contrast to the effect of vacancies on the hardness in B2 compounds, where vacancies are a potent hardener. The vacancy hardening in metals and B2 compounds is often correlated to an interaction between the stress field of a moving dislocation and that of the vacancy. The effect of vacancies in Laves phases is different from their effects in metals and B2 compounds. This is again believed to be due to the fact that Laves phases have a topologically close-packed structure and it is impossible for ordinary dislocations to move in Laves phases. The presence of vacancies in Laves phases would make the structure less closely packed and could possibly assist the synchroshear deformation of the alloy [33], thus leading to the softening of the alloys.

4.4 Fracture Toughness in Binary Laves Phases

The fracture toughness of the alloys does not change as a function of stoichiometry, indicating that the anti-site defect does not significantly affect the deformability and fracture toughness of the materials.

It has been suggested that vacancies in Laves phases may assist the synchroshear mechanism, thus leading to improvement in the deformability and toughness of the Laves alloys [33]. Chen et al. [7] attributed the toughness improvement in the off-stoichiometric $TiCr_2$ alloys to the presence of vacancies in the alloys. In this study, we find that the quenched-in thermal vacancies do not affect the crack propagation and fracture toughness behavior of the $NbCr_2$ alloys (Fig. 14). This is possibly due to the level of vacancies is too low in the alloys to enhance toughness significantly. However, the high residual thermal stress after quenching from 1400°C may also embrittle the $NbCr_2$ Laves phases, which could mask the effect of vacancy-assisted sychroshear deformation [34].

More work on point defects in Laves phases should be pursued, with the hope that constitutional vacancies, instead of thermal vacancies, may exist in certain Laves phases. Such systems will be suitable for examining if the vacancy-assisted synchroshear deformation and toughness improvement are possible in Laves phases. It has been found that for the B2 phases, the defect mechanism is closely related to the enthalpies of formation (ΔH) of the compounds. Neumann has demonstrated that B2 compounds with negative ΔH smaller than 75 to 90 kJ/mole generally exhibit the anti-site defect structure, while compounds with a greater value generally exhibit the triple defect structure and have constitutional vacancies on the large atom-rich side of stoichiometry [35]. In other words, constitutional vacancies are the preferred defect mechanism for compounds that are more strongly ordered, i.e., with higher absolute ΔH values on the large atom-rich side. This empirical observation may be extended to the binary Laves phases. The ΔH values for $NbCr_2$, $NbCo_2$, and $NbFe_2$ are -21, -51, and -63 kJ/mole, respectively [36]. These values are in the same range with those of B2 compounds with anti-site defects. It is not

surprising that only anti-site defects are observed for these Laves phases. It will be interesting to study the defect structures of those Laves phases with more negative enthalpy of formation. The possibility of the existence of constitutional vacancies will be higher for these Laves phases. Some examples of Laves phases with such characteristics will be $ZrCo_2$ and $ZrAl_2$ with ΔH equal to -123 and -138 kJ/mole [36]. Research is in progress in our laboratory to determine the defect mechanisms in these Laves phases.

5. CONCLUSIONS

Point defects in the binary $NbCr_2$, $NbCo_2$, and $NbFe_2$ systems have been clarified combining both bulk density and X-ray lattice parameter measurements. The vacancy concentrations in these systems after quenching from 1000°C are essentially zero. The constitutional defects on both sides of stoichiometry for these systems are of the anti-site type. Such defect mechanism is further supported by the change of the lattice parameter as a function of the stoichiometry. As the Nb content in the Laves phases increases, the lattice parameters on the Nb-rich side increase faster than those on the Cr-, Co-, or Fe-rich side.

The previous postulation that constitutional vacancies are the defect mechanism on the Nb-rich side of $NbCr_2$ Laves phase is not confirmed. For the $NbCo_2$ system, it was found that about 0.7% solubility of Nb exists on the Nb-rich side. As in the $NbCr_2$ system, no consitutional vacancy was found for the Nb-rich compound. However, thermal vacancies exhibiting a maximum at the stoichiometric composition were obtained in $NbCr_2$ Laves phase alloys after quenching from 1400°C. These vacancies could be completely eliminated by annealing at 1000°C.

Hardening, presumably due to anti-site defects, was observed on both sides of stoichiometry for all three Laves phase systems studied. Furthermore, the thermal vacancies in $NbCr_2$ alloys after quenching from 1400°C were found to soften the Laves phases. The off-stoichiometric hardening of the Laves phases is similar to that of the B2

compounds, while the thermal vacancy softening is unique to the Laves phase. Both anti-site defects and thermal vacancies do not significantly affect the fracture toughness of the Laves phases.

6. Acknowledgments

This research was jointly sponsored by the Fossil Energy Advanced Research and Technology Development (AR & TD) Materials Program with Dr. R.R. Judkins as the program manager under subcontract 11X-SP173V to the University of Tennessee, and the Division of Materials Sciences, U.S. Department of Energy, under contract DE-AC05-96OR22464 with Lockheed Martin Energy Research Corporation. Additional funding is provided by the Southeast University Research Association (SURA) with Prof. T. Hutchinson as the contract monitor. The authors are very grateful to Joe Wright, Elmer Lee, and Cecil Carmichael at Oak Ridge National Laboratory (ORNL) for their technical assistance. Thanks are also due to J.H. Schneibel and E.P. George of ORNL for reviewing this manuscript.

REFERENCES

1. Laves, F., in *Theory of Alloy Phases*, American Society for Metals, Metals Park, OH, 1956, p. 124.
2. Wernick, J.H., in *Intermetallic Compounds*, ed. J. H. Westbrook, Wiley, New York, 1967, p. 197.
3. Sinha, A.K., *Progr. in Mater. Sci.*, 1972, **15 (Part 2)**, 79.
4. Massalski, T.B., in *Physical Metallurgy Part 1*, ed. R. W. Cahn and P. Hassen, North-Holland Physics Publishing, NY, 1983, p. 190.
5. Thoma, D. J. and Perepezko, J. H., *J. of Alloys and Compounds*, 1995, **224**, 330.

6. Hazzledine, P. M., Kumar, K. S., Miracle, D. B., and Jackson, A. G., *MRS Symp. Proc.*, 1992, **288**, 591.

7. Chen, K. C., Allen, S. M., and Livingston, J. D., *MRS Symp. Proc.*, 1994, **364**, 1406.

8. Ivey, D.G. and Northwood, D.O., *Z. Phys. Chem. N. F.*, 1986, **147**, 191.

9. Sicking, G., Magomedbekov, E., Hempelmann, R., *Ber. Bunsenges. Phys. Chem.*, 1981, **85**, 686.

10. Takeyama, M. and Liu, C. T. *Mater. Sci. & Eng.*, 1991, **A132**, 61.

11. Cook, J. A., Liaw, P. K., and Liu, C. T., in *Fatigue and Fracture of Ordered Intermetallics*, ed. W.O. Soboyejo, T.S. Srivatsan, and R.O. Ritchie, TMS, Warrendale, PA, 1995, p. 155.

12. Chan, K. S. and Davidson, D. L., *JOM*, 1996, **48**, 62.

13. Thoma, D. J. and Perepezko, J. H., *Mater. Sci. & Eng.*, 1992, **A156**, 97.

14. Zhu, J. H., Pike, L. M., Liaw, P. K. and Liu, C. T., *Scripta Mater.*, 1998, **39**, 833.

15. Zhu, J. H., Liaw, P. K. and Liu, C. T., *Mater. Sci. Eng.*, 1997, **A239-240**, 260.

16. Saito, S. and Beck, P. A., *Trans. Metall. Soc. AIME*, 1960, **218**, 670.

17. Massalski, T. B., Murray, J. L., Bennett, L. H., and Baker, H., *Binary Alloy Phase Diagrams*, American Society for Metals, Metals Park, Ohio, 1986.

18. Smith, A. W., Rogers, J. A., and Rawlings, R. D., *Phys. Stat. Sol. (a)*, 1973, **15**, K119.

19. Paul, E., and Swartzendruber, L. J., *Bulletin of Alloy Phase Diagrams*, 1986, **7(3)**, 248.

20. Bejarano, J. M. Z., Gama, S., Ribeiro, C. A., and Effenberg, G., *Z. Metallkd.*, 1993, **84(3)**, 160.

21. Dieter, G. E., *Physical Metallurgy*, Third Edition, McGraw-Hill, Inc., 1986, p. 331.

22. Sakai, M. and Bradt, R. C., *Inter. Mater. Rev.*, 1993, **38** (**2**), 53.

23. Anstis, G. R., Chantikul, P., Lawn, B. R., and Marshall, D. B., *J. of Amer. Ceram. Soc.*, 1981, **64**(**9**), 533.

24. Anton, H. and Schmidt, P. C., *Intermetallics*, 1997, **5**, 449.

25. Pike, L. M., Chang, Y. A., and Liu, C. T., *Acta Mater.*, 1997, 45, 3709.

26. Chang, Y. A. and Neumann, J. P., *Progr. Solid State Chem.*, 1982, **14**, 221.

27. Riviere, J. P., *Mat. Res. Bull.*, 1977, **12**, 995.

28. Fleischer, R. L., *Scripta Metall. Mater.*, 1992, **27**, 799.

29. Pargeter, J. K., and Hume-Ruthery, W., *J. Less-Common Met.*, 1967, **12**, 366.

30. Brückner, W, Kleinstück, K., and Schulze, G. E. R., *Phys. Stat. Sol.*, 1967, **23**, 475.

31. Foley, J. C., Thoma, D. J., and Perepezko, J. H., *Metall. Trans.*, 1994, **25A**, 230.

32. Pearson, W. B., *The Crystal Chemistry and Physics of Metals and Alloys*, Wiley, New York, NY, 1972, p.151.

33. Hazzledine, P. M., and Pirouz, P., *Scripta Metall. et Mater.*,1993, **28**, 1277.

34. S. Lee, P. K. Liaw, C. T. Liu, and Y. T. Chou, "Thermal Stresses in In-Situ Cr-$NbCr_2$ Composite", to be submitted to Mater. Sci. and Eng., 1998.

35. Neumann, J. P., *Acta Metall.*, 1980, **28**, 1165.

36. de Boer, F. R., Boom, R., Mattens, W. C. M., Miedema, A. R., and Niessen, A. K., *Cohesion in Metals Transition Metal Alloys*, ed. F. R. de Boer and D. G. Pettifor, vol. 1, Second Corrected Printing, North Holland Physics Publishing, Amsterdam, 1989.

Table I Composition, lattice parameter, X-ray density, bulk density, and vacancy concentration (c_V) of the $NbCr_2$ alloys quenched from 1400 and 1000°C

Alloy Code	Nb (at.%)	Lattice Parameter (Å)		X-Ray Density (g/cm^3)		Bulk Density (g/cm^3)		c_V (%)	
		1400°C	1000°C	1400°C	1000°C	1400°C	1000°C	1400°C	1000°C
#1	31.8	6.9843*	6.9861*	---	---	7.613	7.621	---	---
#2	32.3	6.9861	6.9862*	7.619	---	7.617	7.623	0.03	---
#3	32.8	6.9882	6.9884	7.636	7.635	7.623	7.636	0.17	0.03
#4	33.3	6.9904	6.9908	7.652	7.651	7.627	7.646	0.33	0.07
#5	33.8	6.9956	6.9954	7.659	7.660	7.646	7.655	0.17	0.06
#6	34.8	7.0063	7.0063	7.671	7.671	7.664	7.672	0.10	0.00

* Two-phase alloys with the lattice parameter of the $NbCr_2$ phase listed here

Table II Composition, lattice parameter, X-ray density, bulk density, and vacancy concentration (c_V) of the $NbCo_2$ alloys quenched from 1000°C

Alloy Code	Nb (at.%)	Lattice Parameter (Å)	X-Ray Density (g/cm^3)	Bulk Density (g/cm^3)	c_V (%)
#1	27.3	6.7265	---	---	---
#2	29.3	6.7450	---	---	---
#3	31.3	6.7641	8.951	8.950	0.02
#4	33.3	6.7824	8.966	8.967	-0.01
#5	33.8	6.7884	8.964	8.963	0
#6	34.3	6.7917*	---	---	---

* Two-phase alloys with the lattice parameter of the $NbCo_2$ phase listed here

Table III Composition, lattice parameter, X-ray density, bulk density, and vacancy concentration (c_V) of the $NbFe_2$ alloys quenched from 1000°C

Alloy Code	Nb (at.%)	Lattice Parameter (Å)		X-Ray Density (g/cm^3)	Bulk Density (g/cm^3)	c_V (%)
		a	c			
#1	32.3	4.8363	7.8919	8.449	8.444	0.07
#2	32.8	4.8378	7.8936	8.465	8.462	0.04
#3	33.3	4.8406	7.8966	8.474	8.470	0.06
#4	33.8	4.8446	7.9030	8.478	8.472	0.07
#5	34.3	4.8504	7.9093	8.473	8.469	0.06
#6	36.3	4.8601*	7.9147*	---	---	---
#7	37.3	4.8602*	7.9146*	---	---	---

* Two-phase alloys with the lattice parameter of the $NbFe_2$ phase listed here

Captions

Fig. 1 (a) Optical microstructure of the stoichiometric $NbCr_2$ alloy after quenching from 1000°C (in the etched condition); (b) SEM micrograph of the $NbCr_2$ alloy #1 after quenching from 1000°C (in the as-polished condition); (c) EDS spectra of the matrix and the dark phase indicated in (b), which were $NbCr_2$ Laves phases and Cr precipitate, respectively.

Fig. 2 (a) Optical microstructure of the stoichiometric $NbCo_2$ alloy; (b) SEM micrograph of the $NbCo_2$ alloy #6. Both in the etched condition.

Fig. 3 (a) Optical microstructure of the stoichiometric $NbFe_2$ alloy; (b) SEM micrograph of the $NbFe_2$ alloy #7. Both in the etched condition.

Fig. 4 Lattice parameter as a function of the Nb content for $NbCr_2$ alloys after quenching from 1400 and 1000°C.

Fig. 5 X-ray and bulk densities as a function of the Nb content for $NbCr_2$ alloys after quenching from 1400 and 1000°C.

Fig. 6 Vacancy concentration as a function of the Nb content for $NbCr_2$ alloys after quenching from 1400 and 1000°C.

Fig. 7 Lattice parameter as a function of the Nb content for $NbCo_2$ alloys after quenching from 1000°C.

Fig. 8 X-ray and bulk densities as a function of the Nb content for $NbCo_2$ alloys after quenching from 1000°C.

Fig. 9 Lattice parameters, a and c, as a function of the Nb content for $NbFe_2$ alloys after quenching from 1000°C.

Fig. 10 X-ray and bulk densities as a function of the Nb content for $NbFe_2$ alloys after quenching from 1000°C.

Fig. 11 Vickers Hardness versus Nb content for $NbCr_2$ alloys after quenching from 1400°C and 1000°C.

Fig. 12 Vickers Hardness versus Nb content for $NbCo_2$ alloys after quenching from 1000°C.

Fig. 13 Vickers Hardness versus Nb content for $NbFe_2$ alloys after quenching from 1000°C

Fig. 14 Fracture toughness versus Nb content for binary $NbCr_2$, $NbCo_2$ and $NbFe_2$ Laves-phase alloys. Note two of the $NbFe_2$ alloys are not single Laves phase.

Fig. 15 Measured vacancy concentration versus Nb content in the binary $NbCr_2$, $NbCo_2$ and $NbFe_2$ Laves phases after quenching from 1000°C. Also shown are the calculated data for the constitutional vacancy model and the anti-site substitution model.

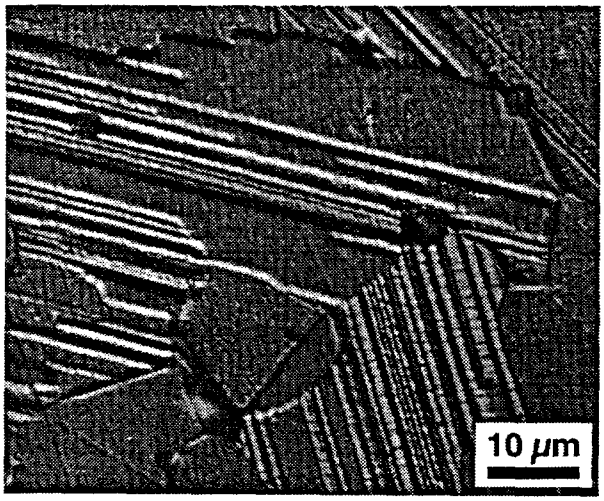
10 μm

(a)

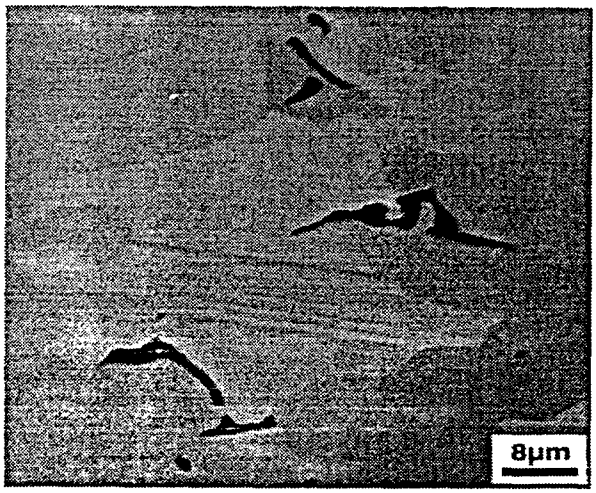
8μm

(b)

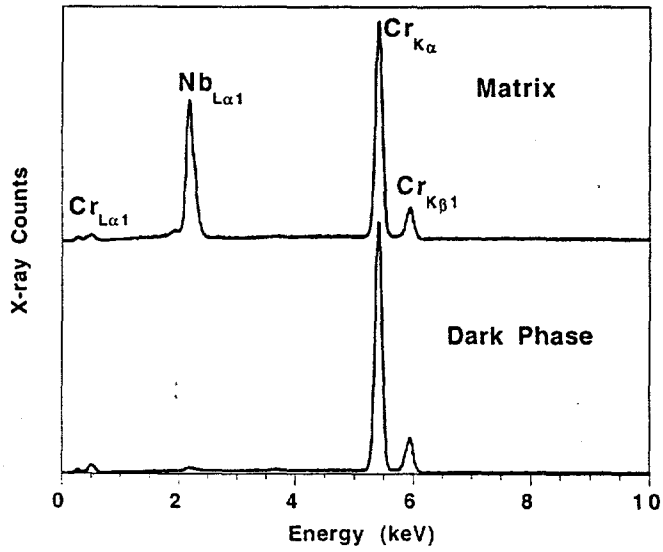
Cr Kα
Nb Lα1
Matrix
Cr Lα1
Cr Kβ1
Dark Phase
X-ray Counts
0
2
4
6
8
10
Energy (keV)

(c)

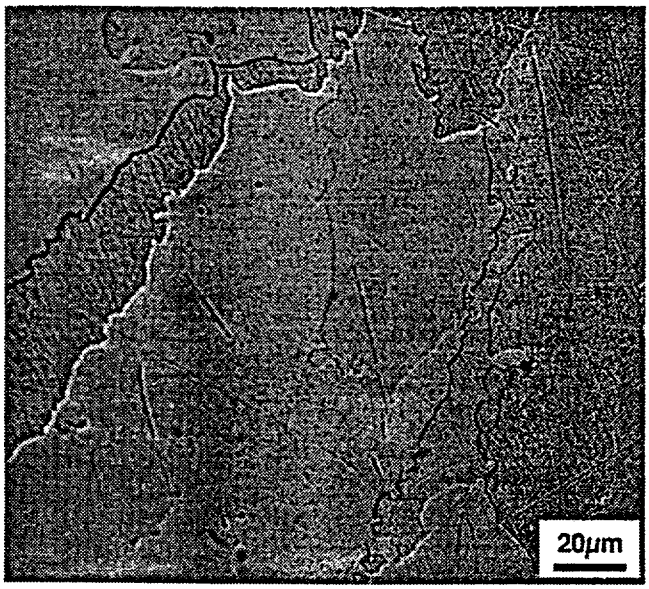

(a)

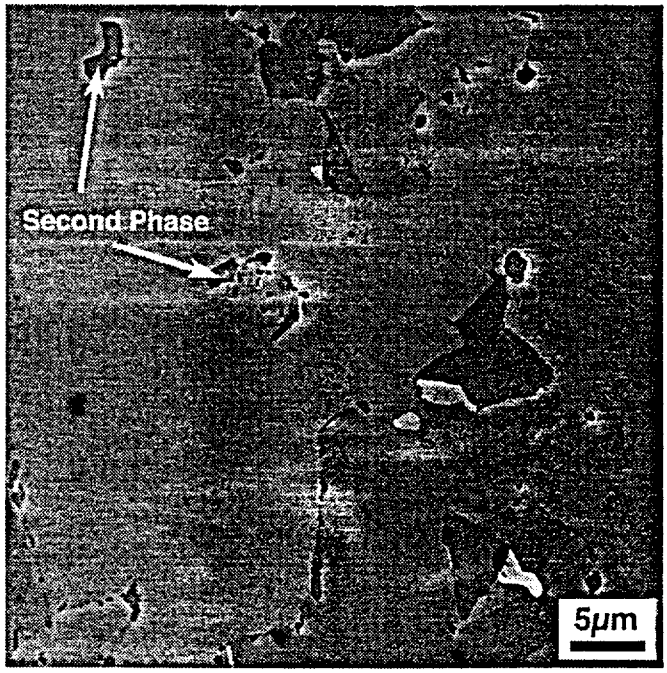

(b)

(Fig. 2)

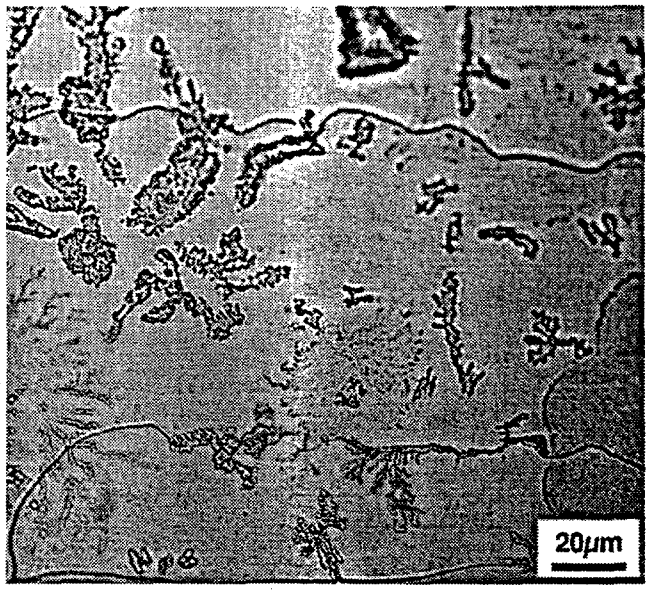

(a)

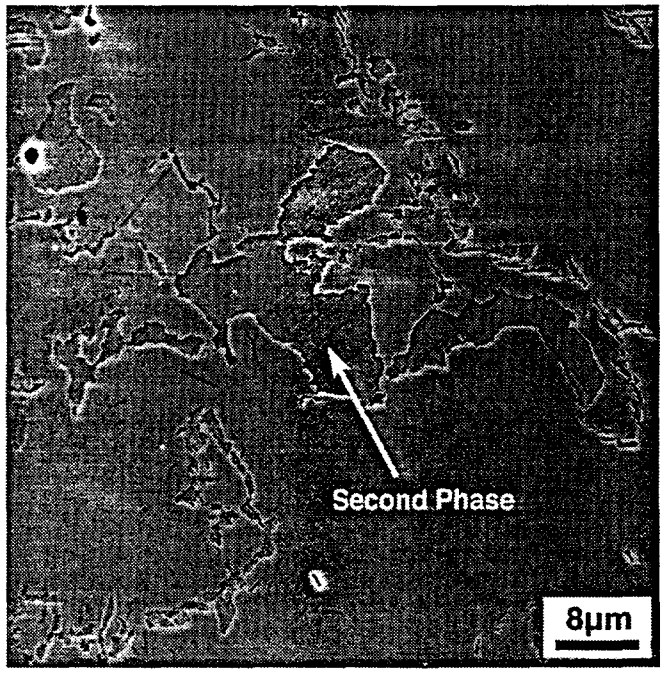

(b)

(Fig. 3)

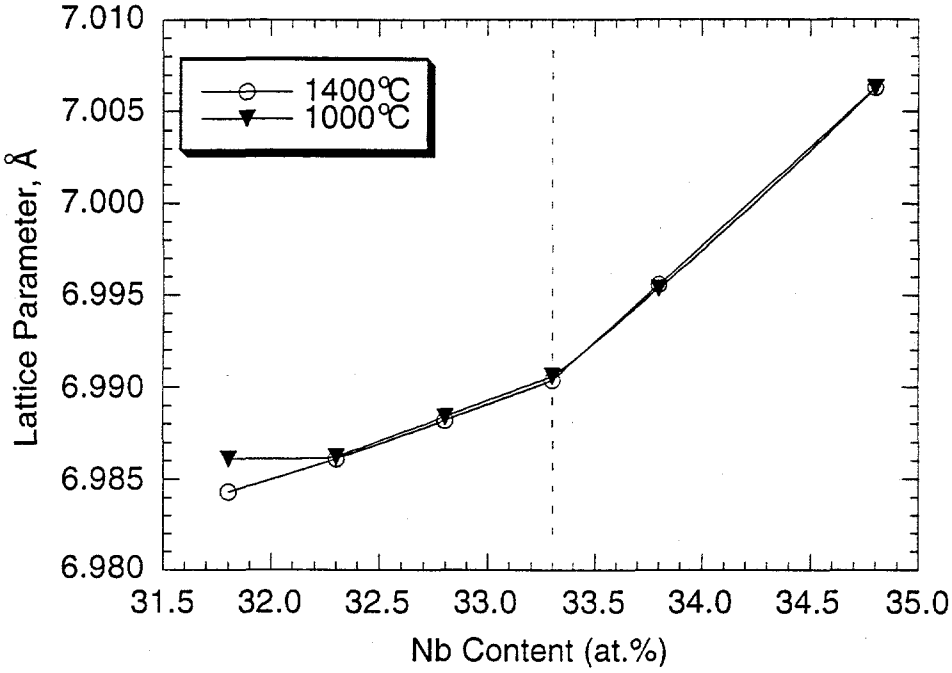

Fig. 4 Lattice parameter as a function of the Nb content for $NbCr_2$ alloys alloys after quenching from 1400 and 1000°C

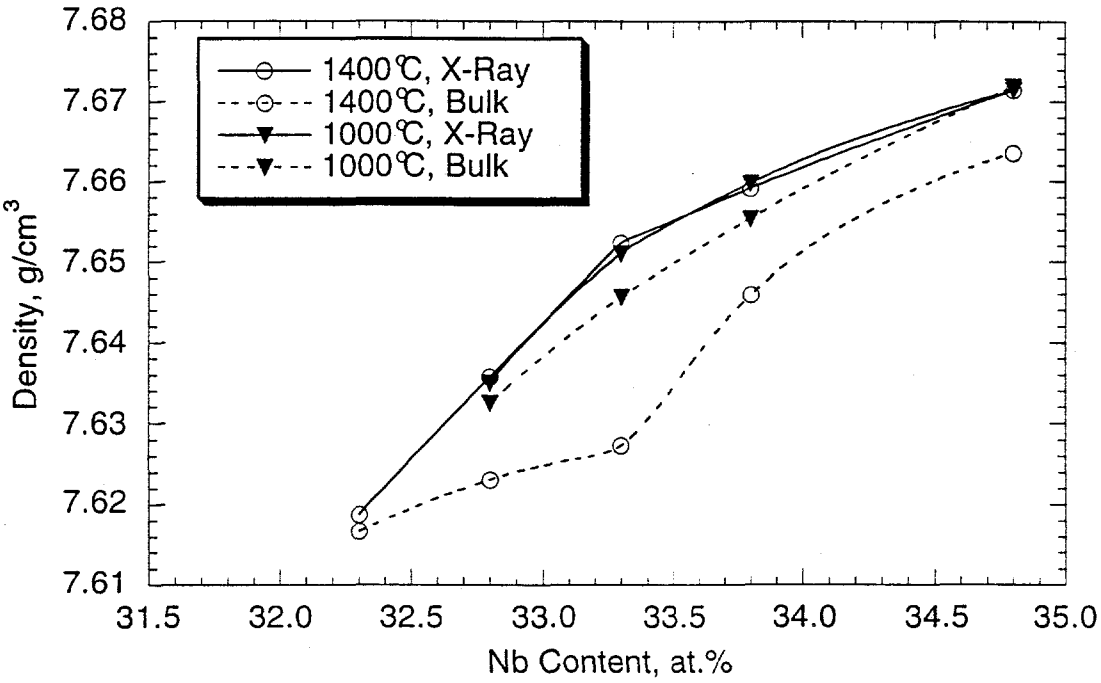

Fig. 5 X-ray and bulk densities as a function of the Nb content for $NbCr_2$ alloys after quenching from 1400 and 1000°C

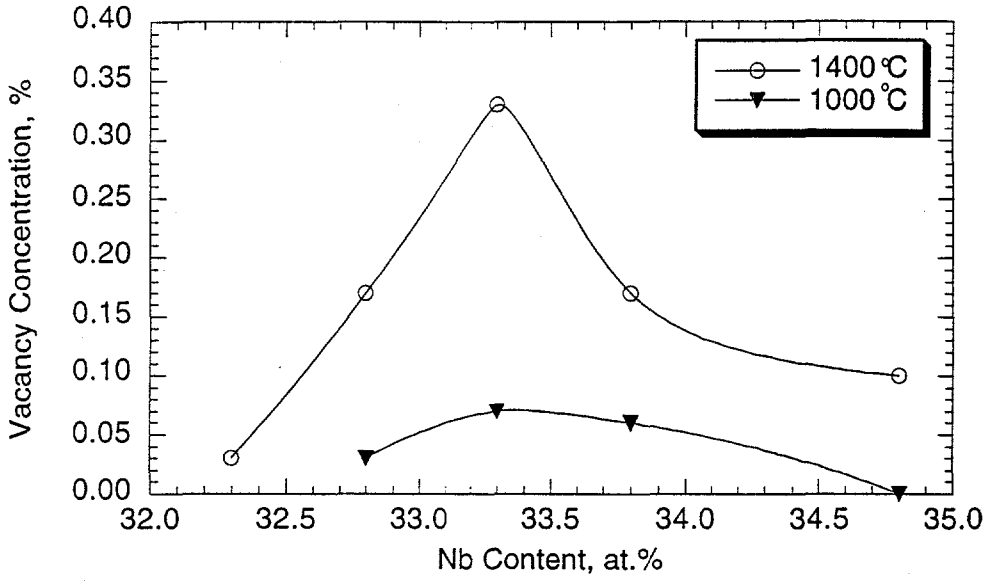

Fig. 6 Vacancy concentration as a function of the Nb content for $NbCr_2$ alloys after quenching from 1400 and 1000°C

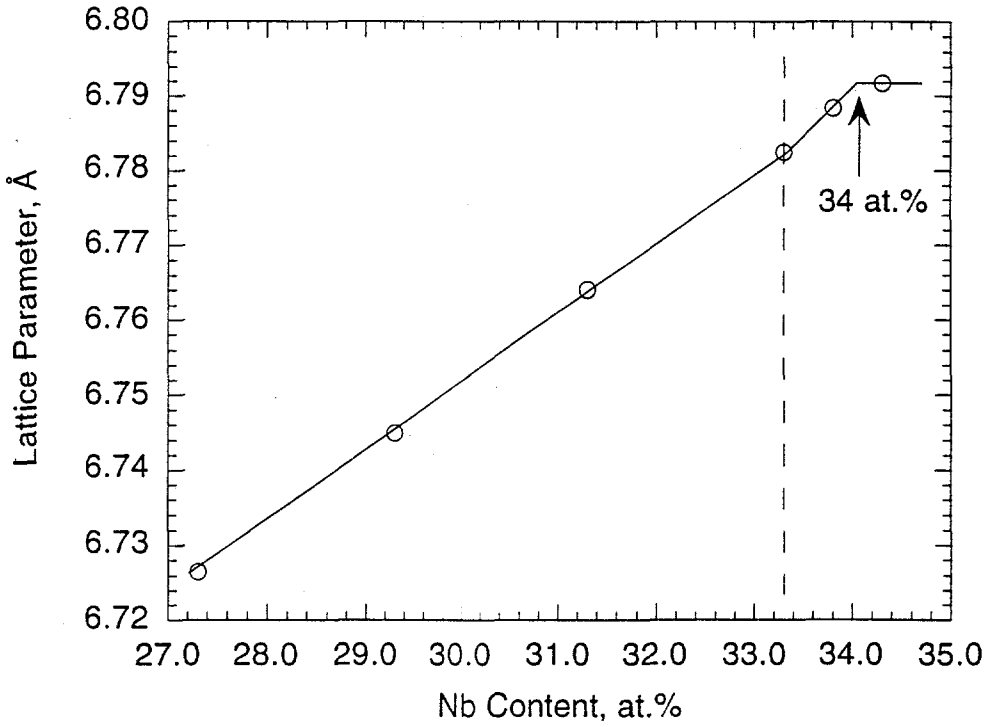

Fig. 7 Lattice parameter as a function of the Nb content for $NbCo_2$ alloys alloys after quenching from 1000°C

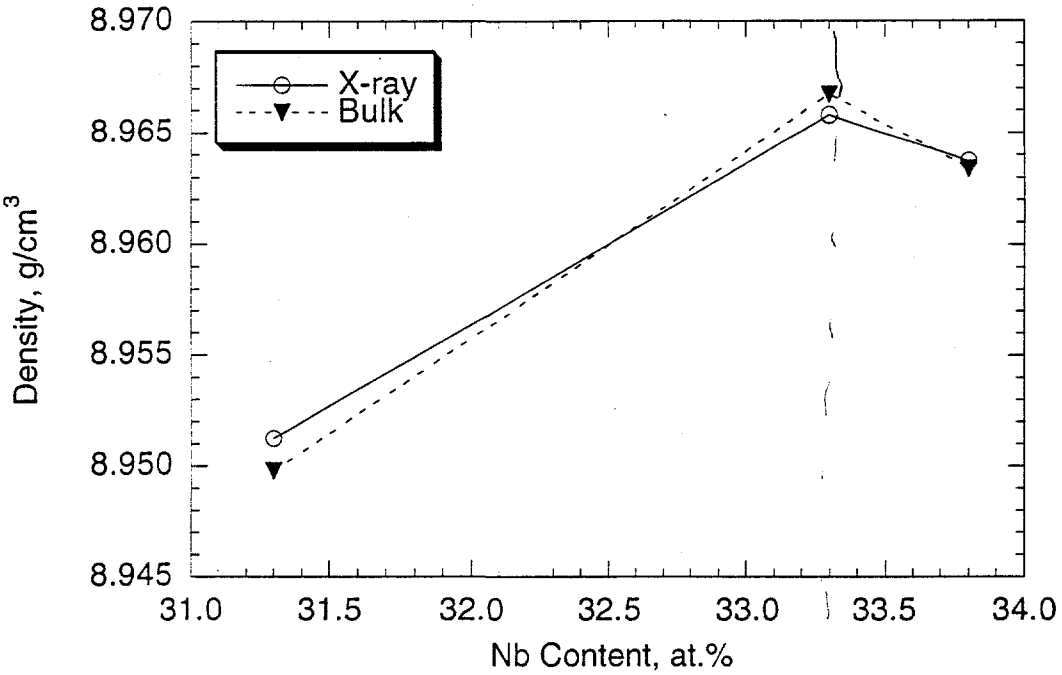

Fig. 8 X-ray and bulk densities as a function of the Nb content for $NbCo_2$ alloys alloys after quenching from 1000°C

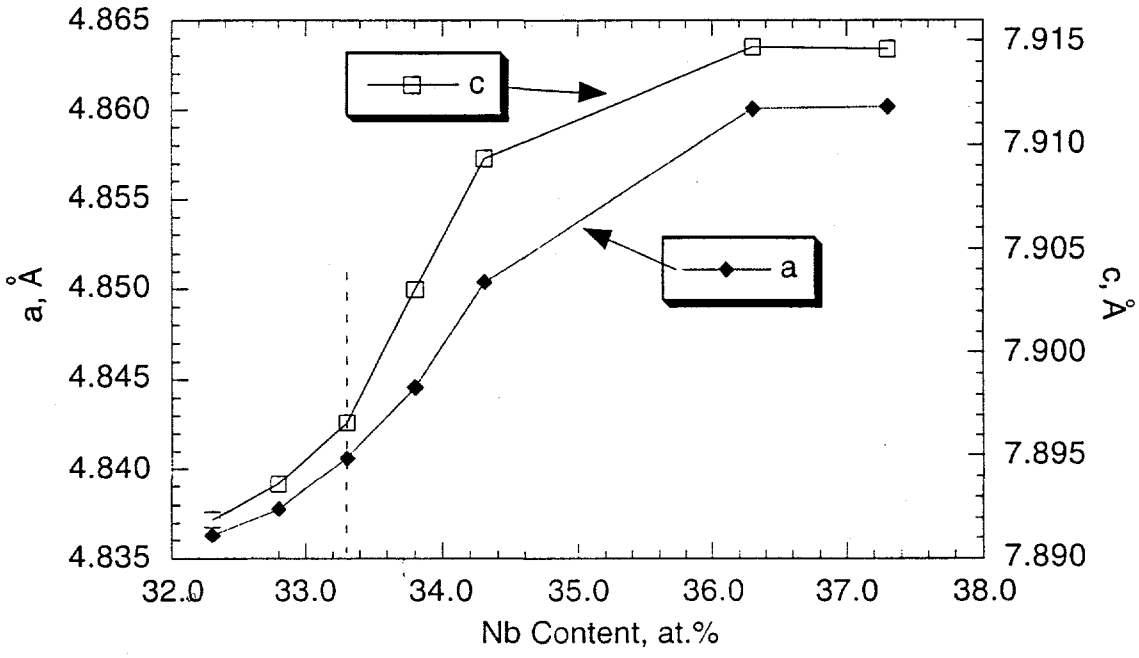

Fig. 9 Lattice parameters, a and c, as a function of Nb content for $NbFe_2$ alloys alloys after quenching from 1000°C

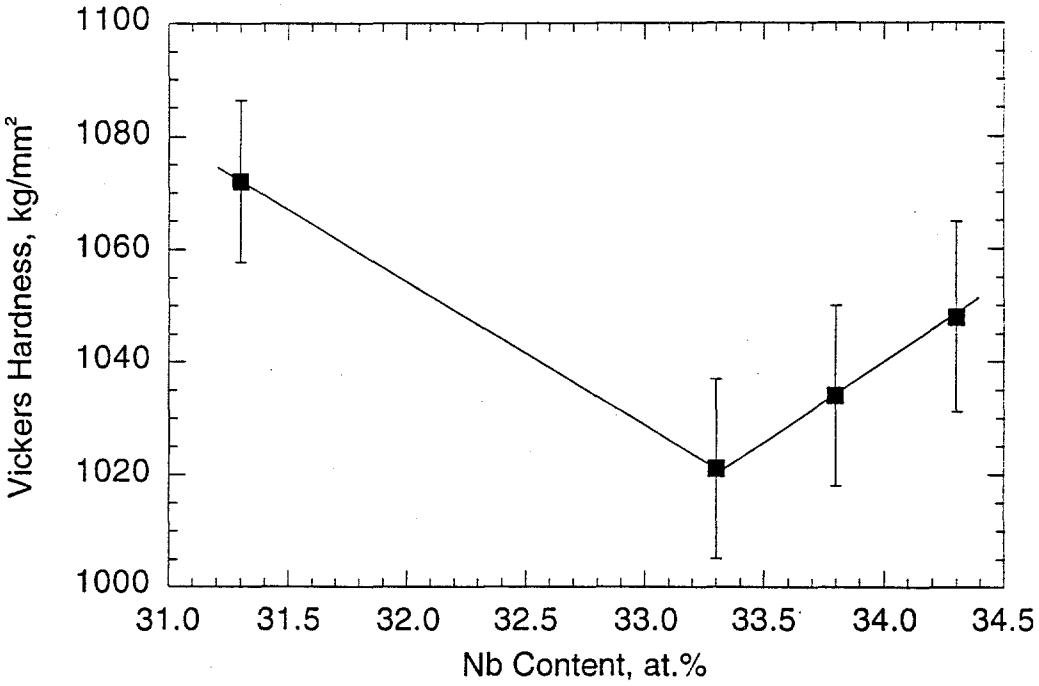

Fig. 12 Vickers Hardness versus Nb content for $NbCo_2$ alloys after quenching from 1000°C

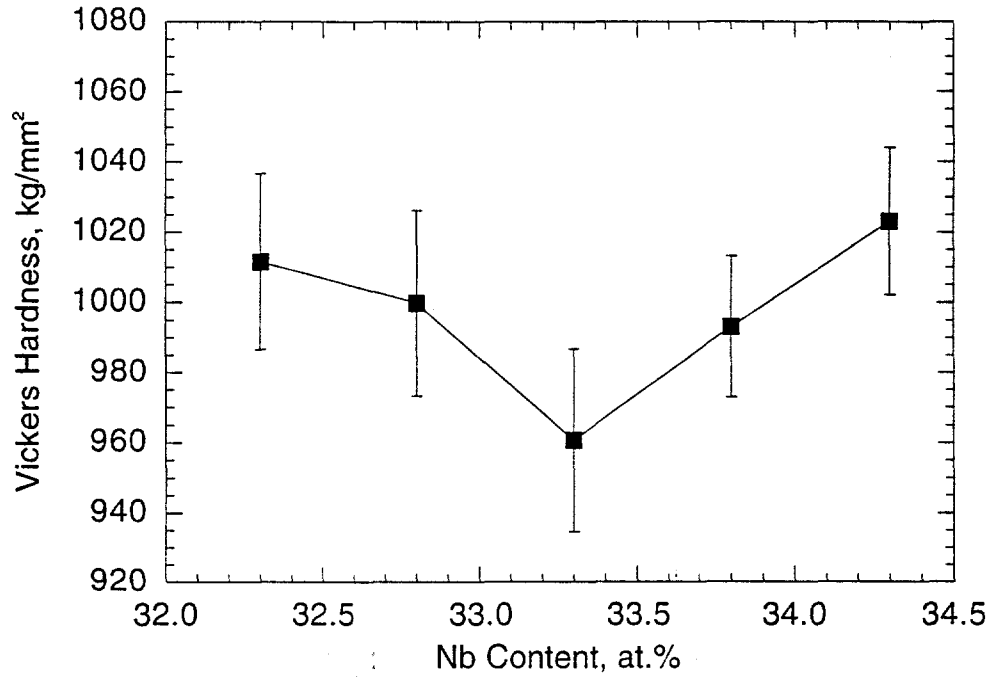

Fig. 13 Vickers Hardness versus Nb content for $NbFe_2$ alloys after quenching from 1000°C

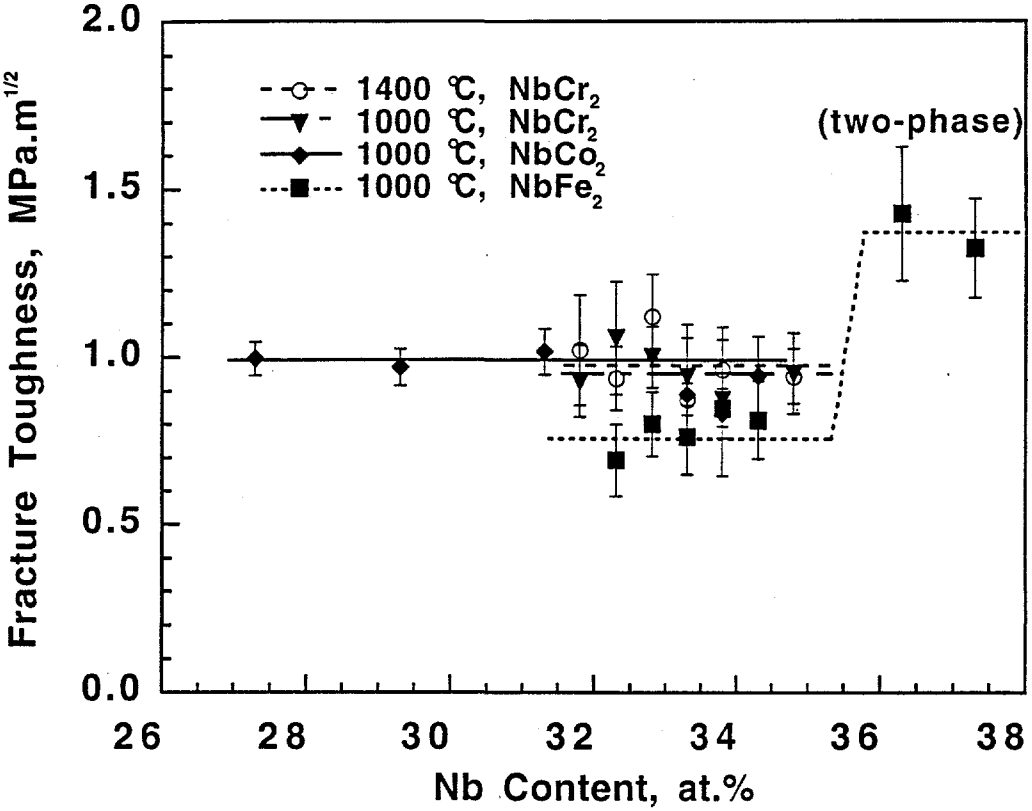
2.0
1.5
1.0
0.5
0.0
Fracture Toughness, MPa.m$^{1/2}$
1400 ℃, $NbCr_2$
1000 ℃, $NbCr_2$
1000 ℃, $NbCo_2$
1000 ℃, $NbFe_2$
(two-phase)
26
28
30
32
34
36
38
Nb Content, at.%

(Fig. 14)

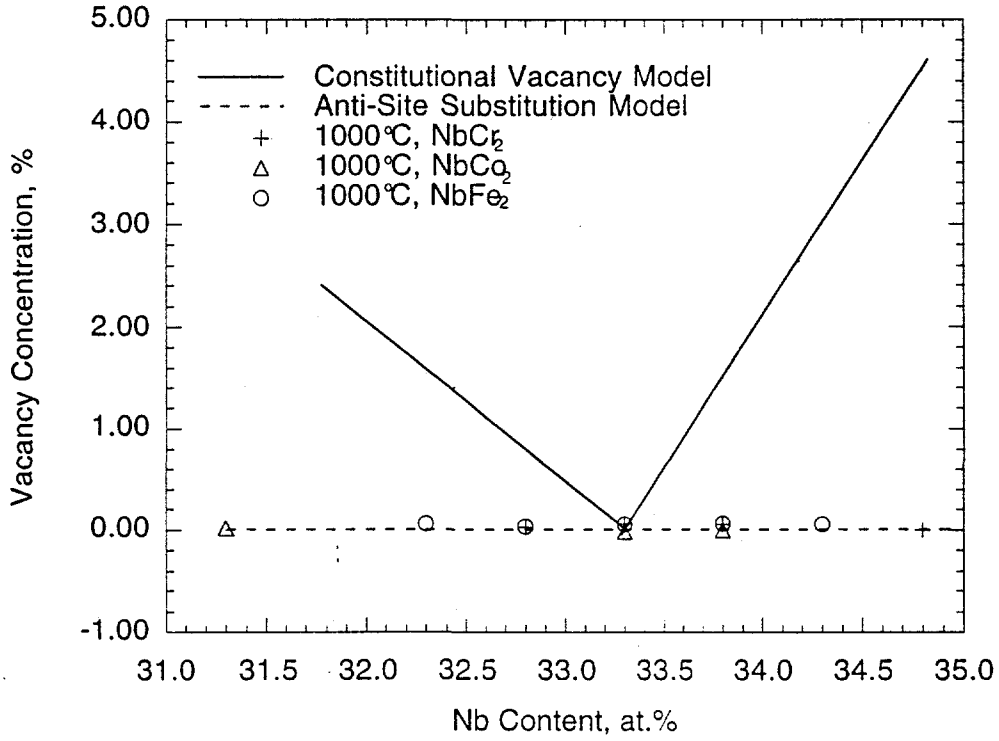
5.00
4.00
3.00
2.00
1.00
0.00
-1.00
Vacancy Concentration, %
Constitutional Vacancy Model
Anti-Site Substitution Model
1000℃, $NbCr_2$
1000℃, $NbCo_2$
1000℃, $NbFe_2$
31.0
31.5
32.0
32.5
33.0
33.5
34.0
34.5
35.0
Nb Content, at.%

(Fig. 15)

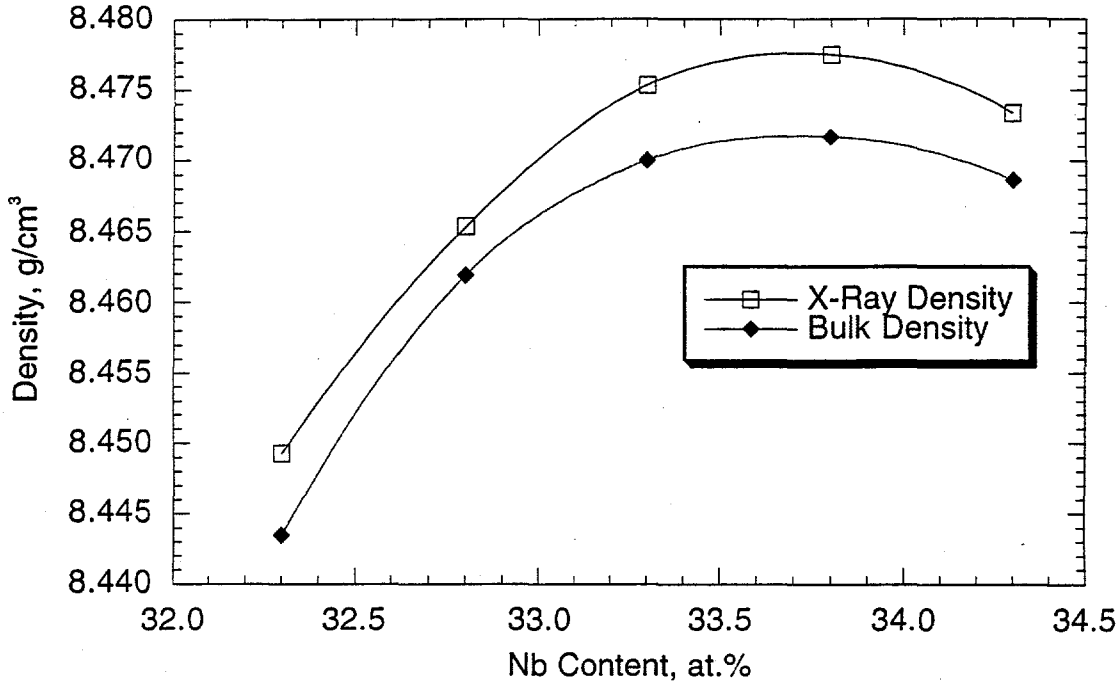

Fig. 10 X-ray and bulk densities as a function of Nb content for $NbFe_2$ alloys

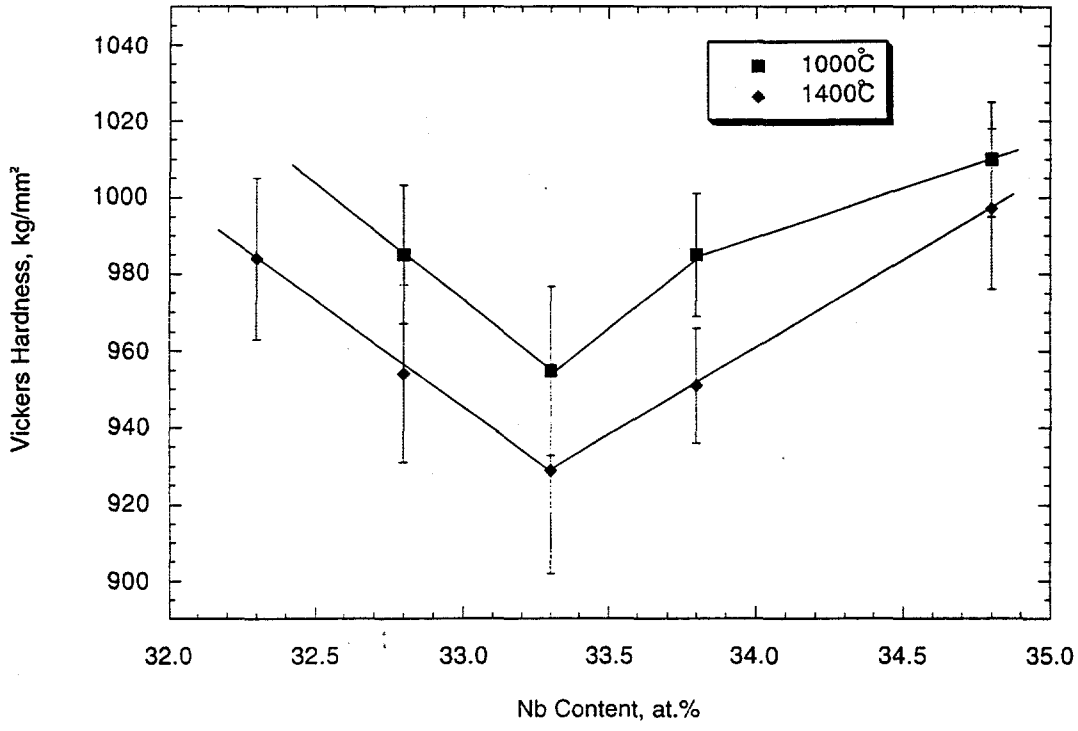

Fig. 11 Vickers Hardness versus Nb content for $NbCr_2$ alloys after quenching from 1400°C and 1000°C